Bimetallic single-source precursors [M(NH 3) 4][Co(C 2O 4) 2(H 2O) 2]·2H 2O (M = Pd, Pt) for the one run synthesis of CoPd and CoPt magnetic nanoalloys

ARTICLE *in* POLYHEDRON · APRIL 2011

Impact Factor: 2.01 · DOI: 10.1016/j.poly.2011.02.012

8 AUTHORS, INCLUDING:

Andrey V. Zadesenets
Russian Academy of Sciences
24 PUBLICATIONS **102** CITATIONS
SEE PROFILE

Evgeny Yurievich Filatov
Russian Academy of Sciences
29 PUBLICATIONS **121** CITATIONS
SEE PROFILE

Pavel E. Plyusnin
Russian Academy of Sciences
59 PUBLICATIONS **149** CITATIONS
SEE PROFILE

Artem S. Bogomyakov
Russian Academy of Sciences
155 PUBLICATIONS **618** CITATIONS
SEE PROFILE

Polyhedron 30 (2011) 1305–1312

Contents lists available at ScienceDirect

Polyhedron

journal homepage: www.elsevier.com/locate/poly

Bimetallic single-source precursors $[M(NH_3)_4][Co(C_2O_4)_2(H_2O)_2]\cdot 2H_2O$ (M = Pd, Pt) for the one run synthesis of CoPd and CoPt magnetic nanoalloys

Andrey Zadesenets [a,b,*], Evgeny Filatov [a,b], Pavel Plyusnin [a,b], Iraida Baidina [a], Vasiliy Dalezky [a], Yuri Shubin [a,b], Sergey Korenev [a,b], Artyom Bogomyakov [c]

[a] Nikolaev Institute of Inorganic Chemistry SB RAS, Lavrentyev Ave. 3, 630090 Novosibirsk, Russia
[b] Novosibirsk State University, Pirogov St. 2, 630090 Novosibirsk, Russia
[c] International Tomography Center SB RAS, Institutskaya Str. 3A, 630090 Novosibirsk, Russia

ARTICLE INFO

Article history:
Received 20 January 2011
Accepted 9 February 2011
Available online 23 February 2011

Keywords:
Cobalt
Platinum
Palladium
Heterometallic complexes
Thermochemistry
Single-source precursors
Nanoalloys
Magnetic properties

ABSTRACT

All the steps of the proposed technique, from the synthesis of single-source precursors to the preparation of CoPd and CoPt nanoalloys, are described. The double complex salts (DCS) $[M(NH_3)_4][Co(C_2O_4)_2(H_2O)_2]\cdot 2H_2O$ (M = Pd, Pt), which were synthesized by mixing solutions containing $[M(NH_3)_4]^{2+}$ cations and $[Co(C_2O_4)_2(H_2O)_2]^{2-}$ anions, have been used as precursors. The salts obtained were characterized by IR spectroscopy, thermal analysis, XRD and single crystal X-ray diffraction. The prepared compounds crystallize in the monoclinic (space group *I*2/*m*, M = Pd) and orthorhombic (space group *I*222, M = Pt) crystal systems. Thermal decomposition of the salts in helium or hydrogen atmosphere at 200–600 °C results in the formation of nanoalloys powders (random solid solution $Co_{0.50}Pd_{0.50}$ and chemically ordered CoPt). The size of the bimetallic particles varied from 5 to 20 nm. Order–disorder structural transformations in $Co_{0.50}Pt_{0.50}$ nanoalloys were studied. The magnetic properties of both chemically disordered $Co_{0.50}Pd_{0.50}$ and ordered CoPt clusters have also been measured.

1. Introduction

Ultrafine bimetallic powders are currently attracting significant interest from researchers active in various fields of chemistry [1,2]. These systems possess unique electrical, chemical, structural and magnetic properties because of the large fraction of surface atoms and because of the finite number of atoms in each crystalline core. A considerable number of works attract great attention to the systems Co–Pd and Co–Pt, due to their high catalytic activities [3–7] and outstanding magnetic characteristics [8–11].

Currently, there is a great variety of synthetic approaches to nanoalloy fabrication. The most popular techniques are the colloidal method [12–16] and decomposition of individual precursor compounds [17]. Practically in all cases, two individual precursors of each metal are used. For example, CoPt nanoparticles were synthesized by the chemical reduction of $Co(CH_3COO)_2$ and $Pt(acac)_2$ by polyethyleneglycol-200 [18].

We report a simple chemical process for the synthesis of Co–Pd and Co–Pt nanoparticles by a one run reduction of a single-source precursor, having both metals in the one compound. The initial atomic ratio of the metals in the precursors is carried over to the final product, and the equimolecular composition is easily tuned. The advantages of this approach are illustrated in the literature [19,20]. In these studies, DCS's containing platinum/palladium with chromium, iron, nickel, copper and zinc were investigated. Thermal annealing is applied to control the structural and magnetic properties of the assemblies. This controlled synthesis of nanoparticles offers a convenient route for the fabrication of Co–Pd and Co–Pt nanoparticle-based devices.

In this work, we synthesized the single-source precursors $[M(NH_3)_4][Co(C_2O_4)_2(H_2O)_2]\cdot 2H_2O$ (M = Pd, Pt). The main goals of this study are the examination of structure, thermal properties of the compounds, phase composition and properties of the metallic products.

2. Experimental

2.1. Syntheses of the precursors

The starting compounds $[M(NH_3)_4]Cl_2$ (M = Pd, Pt) were prepared from metallic platinum/palladium by the standard technique [21]. The anionic salt $(NH_4)_2[Co(C_2O_4)_2(H_2O)_2]$ was prepared only in solution. A concentrated solution of $Co(NO_3)_2$ (1.1 mmol) was added to a concentrated $(NH_4)_2C_2O_4$ solution (2.4 mmol). The color of the solution turned from purple to pink, indicating the formation

* Corresponding author at: Nikolaev Institute of Inorganic Chemistry SB RAS, Lavrentyev Ave. 3, 630090 Novosibirsk, Russia.
E-mail address: zadesenets@ngs.ru (A. Zadesenets).

0277-5387/$ - see front matter © 2011 Elsevier Ltd. All rights reserved.
doi:10.1016/j.poly.2011.02.012

of the $[Co(C_2O_4)_2(H_2O)_2]^{2-}$ complex. Then, a concentrated solution of $[M(NH_3)_4]Cl_2$ (1 mmol) was immediately mixed (to prevent CoC_2O_4 precipitation) with the solution of $(NH_4)_2[Co(C_2O_4)_2(H_2O)_2]$. After that, the solution was cooled to 0 °C, the precipitate of the resulting DCS was collected by filtration, washed with ethanol and dried in air. Elemental (CHN) analysis was carried out with an Euro EA 3000 analyzer. Analysis of metal content is described below in Section 2.4.

$[Pd(NH_3)_4][Co(C_2O_4)_2(H_2O)_2]\cdot 2H_2O$ ([**Pd–Co**]): yield 80%. *Anal.* Calc. for $C_4H_{20}N_4O_{12}PdCo$: C, 9.98; H, 4.19; N, 11.63; (Pd + Co), 34.32. Found: C, 10.2; H, 4.0; N, 11.2; (Pd + Co), 34.2%. Selected IR spectral data (KBr, cm^{-1}): 3283s ($\nu(NH_3)$), 1648s ($\nu_7(C_2O_4^{2-})$), 1434m ($\nu_2(C_2O_4^{2-})$), 1301s ($\nu_8(C_2O_4^{2-})$), 851m ($\rho_r(NH_3)$), 786m ($\nu_9(C_2O_4^{2-})$), 729m ($\nu_9(C_2O_4^{2-})$), 505sh ($\nu_4 + \nu_{10}(C_2O_4^{2-})$), 485m ($\nu_{11}(C_2O_4^{2-})$), 388w ($\nu_5(C_2O_4^{2-})$).

$[Pt(NH_3)_4][Co(C_2O_4)_2(H_2O)_2]\cdot 2H_2O$ ([**Pt–Co**]): yield 85%. *Anal.* Calc. for $C_4H_{20}N_4O_{12}PtCo$: C, 8.42; H, 3.54; N, 9.83; (Pt + Co), 44.54. Found: C, 8.3; H, 3.4; N, 9.3; (Pt + Co), 44.2%. Selected IR spectral data (KBr, cm^{-1}): 3270s ($\nu(NH_3)$), 1650s ($\nu_7(C_2O_4^{2-})$), 1434m ($\nu_2(C_2O_4^{2-})$), 1354s ($\delta_a(NH_3)$), 1301s ($\nu_8(C_2O_4^{2-})$), 903m ($\rho_r(NH_3)$), 784m ($\nu_9(C_2O_4^{2-})$), 725m ($\nu_9(C_2O_4^{2-})$), 515w (ν(Pt–N)), 490m ($\nu_{11}(C_2O_4^{2-})$), 389w ($\nu_5(C_2O_4^{2-})$).

2.2. Single crystal X-ray diffraction analysis

Pink needle crystals of the DCS's were obtained in a U-shaped tube filled with agarose gel. The single crystal X-ray diffraction study was carried out on a BRUKER X8 APEX CCD diffractometer at room temperature using graphite-monochromated Mo Kα radiation (λ = 0.7107 Å). The structures were solved by the standard heavy atom method and refined in anisotropic approximation. All calculations were performed with the SHELX97 program package [22]. Crystal data and experimental details are given in Table 1, selected bond lengths and angles are listed in Table 2, the shortest H-bond contacts are listed in Table 3.

2.3. XRD

Polycrystalline samples were studied over the 2θ range 5–120° on a DRON RM4 powder diffractometer equipped with a Cu Kα source (λ = 1.5418 Å) and a graphite monochromator for the diffracted beam. Indexing of the diffraction patterns was done using data for the pure metals and compounds reported in the JCPDS-ICDD database [23]. Unit cell parameters were refined by full-profile analysis within the whole diffraction range with the POWDERCELL 2.4 program [24]. Crystallite sizes in the prepared bimetallic powders were determined by Fourier analysis of single diffraction peaks (the program WINFIT 1.2.1 [25]).

Determination of the bimetallic phase compositions was based on additive dependence of the specific atomic volume (V/Z) in the solid solutions using calibration curves of V/Z versus x (V – cell volume, Z – atoms number in the one cell, x – composition atomic %). The calibration curves (Fig. 1) were based on the experimental data for cobalt–platinum and cobalt–palladium solid solutions reported in the literature [26,27].

Table 1
Crystal data and experimental details for $[M(NH_3)_4][Co(C_2O_4)_2(H_2O)_2]\cdot 2H_2O$ (M = Pd, Pt).

	Double complex salt	
	[**Pd–Co**]	[**Pt–Co**]
Empirical formula	$C_4H_{20}N_4CoO_{12}Pd$	$C_4H_{20}N_4CoO_{12}Pt$
Formula weight	473.51	570.26
Crystal system	monoclinic	orthorhombic
Space group	*C*12/*m*1	*I*222
a (Å)	10.034(1)	7.1635(4)
b (Å)	7.090(1)	7.2058(3)
c (Å)	15.060(1)	15.1235(9)
Z	2	2
V (Å^3)	769.4(2)	780.66(7)
D_{calc} (g cm^{-3})	2.044	2.426
μ (mm^{-1})	2.312	10.078
F(0 0 0)	466	546
θ Range	3.1–26.4	2.7–30.5
Reflections collected	794	3510
Independent reflections	762	1201
Parameters	57	74
Goodness-of-fit (GOF)	1.149	1.139
R_1, wR ($I > 2\sigma(I)$)]	0.0379, 0.0997	0.0099, 0.0238
R_1, wR (all data)	0.0396, 0.1018	0.0099, 0.0238
Δ_{max}, Δ_{min} (e Å^{-3})	1.910, −0.783	0.662, −0.302

Table 2
Selected bond distances and angles for $[M(NH_3)_4][Co(C_2O_4)_2(H_2O)_2]\cdot 2H_2O$ (M = Pd, Pt).

Distances (Å)		Angles (°)			
[**Pd–Co**]					
Pd–N1	2.045(4)	N1″–Pd–N1	178.62(8)	O1–Co–O1‴	99.7(2)
Co–O1W	2.053(5)	N1–Pd–N1′	91.61(8)	O1–Co–O1′	80.3(2)
Co–O1	2.083(3)	N1″–Pd–N1′	88.40(8)	C1–O1–Co	113.8(3)
O1–C1	1.268(6)	O1W–Co–O1W′	180.0(3)	O2–C1–O1	127.3(4)
O2–C1	1.229(6)	O1W–Co–O1	87.2(2)	O2–C1–C1′	116.9(3)
C1–C1′	1.579(9)	O1W′–Co–O1	92.8(2)	O1–C1–C1′	115.8(2)
		O1–Co–O1″	180.00(1)		
[**Pt–Co**]					
Pt–N1	2.052(2)	N1″–Pt–N1	179.5(7)	O1–Co–O1‴	99.88(6)
Co–O1W	2.034(2)	N1–Pt–N1′	91.39(9)	O1–Co–O1′	80.15(6)
Co–O1	2.081(1)	N1″–Pt–N1′	88.61(9)	C1–O1–Co	113.6(1)
O1–C1	1.267(3)	O1W–Co–O1W′	180.0(1)	O2–C1–O1	126.8(2)
O2–C1	1.230(3)	O1W–Co–O1	89.1(5)	O2–C1–C1′	117.0(1)
C1–C1′	1.559(3)	O1W′–Co–O1	90.9(5)	O1–C1–C1′	116.2(2)
		O1–Co–O1″	178.2(11)		

Table 3
Hydrogen bonding illustrated with interatomic distances A···D in the D–H···A system.

Contacts	Salt	
	[**Pd–Co**]	[**Pt–Co**]
Crystallization water–anion interaction		
O1W···O2W	2.746(8)	2.740(2)
O2···O2W	2.691(4)	2.696(2)
Cation–anion interaction		
N1···O1	3.16(1)	3.12(2)
N1···O1′	3.03(9)	3.08(2)
N1···O2	2.99(8)	3.02(1)

2.4. Thermal analysis

The prepared DCS were studied on a Netzsch STA 409 PC Luxx thermoanalyzer, Al_2O_3 powder being used as a standard. The experiments were run in an open alumina crucible in a helium stream at a heating rate of 10 K/min. The final temperatures of the experiments are reported in Table 4. Analysis of thermal data was carried out with Proteus analysis software [28]. In addition, gaseous products of the thermal decomposition were determined with a mass-spectrometer, QMS 100 Series.

2.5. Nanoalloy preparation

To synthesize bimetallic powders in a hydrogen atmosphere, weighted samples of the DCS (~50 mg) were placed in a tubular quartz reactor. Heating was performed in a split furnace at the rate of 20 K/min. After reaching the final temperature (Table 4), samples were kept for 1 h, and then the hydrogen stream was switched

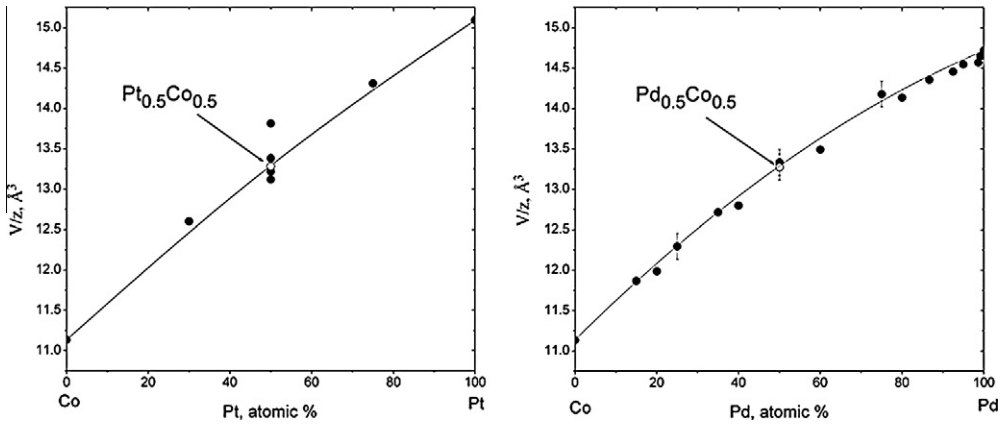

Fig. 1. Calibrated curves for the determination of the nanoalloys' composition. Literature data are shown as filled circles, the data of this work – open circles.

Table 4
Phase composition of the thermolysis products.

Salt-precursor	Atmosphere	t_{max} (°C)	Phase	Space group	*a* (Å)	*c* (Å)	Crystallite size (nm)
[**Pd–Co**]	He	350	$Co_{0.5}Pd_{0.5}$	$Fm\bar{3}m$	3.753(4)		6–8
	H_2	200	Pd + anhydrous DCS	$Fm\bar{3}m$	3.890(3)		6–8
	H_2	400	$Co_{0.5}Pd_{0.5}$	$Fm\bar{3}m$	3.756(3)		12–18
	H_2	600	$Co_{0.5}Pd_{0.5}$	$Fm\bar{3}m$	3.751(2)		18–21
[**Pt–Co**]	He	400	$Co_{0.5}Pt_{0.5}$	$Fm\bar{3}m$	3.749(4)		6–8
	H_2	200	Pt + anhydrous DCS	$Fm\bar{3}m$	3.923(3)		5–7
	H_2	325	$Co_{0.5}Pt_{0.5}$	$Fm\bar{3}m$	3.749(4)		7–9
	H_2	400	CoPt	*P*4/*mmm*	2.677(2)	3.743(3)	10–14
	H_2	600	CoPt	*P*4/*mmm*	2.685(2)	3.693(3)	15–19
	H_2	800	CoPt	*P*4/*mmm*	2.682(2)	3.675(3)	16–20
	H_2	850	$Co_{0.5}Pt_{0.5}$	$Fm\bar{3}m$	3.749(1)		16–21

off and the system was purged with helium for 0.5 h. Afterwards, the furnace was removed and the reactor was allowed to cool to ambient temperature in a continuous helium stream. The product was weighed.

2.6. Electron microscopy

The surface morphology of the materials were studied using a JEOL JSM 6700F scanning electron microscope equipped with an energy dispersive X-ray analyzer EX-23000BU (EDS), operating at 15 kV. A transmission electron microscopy study of the samples was made on a JEOL JEM-100CX device.

2.7. Magnetic measurements

Magnetic measurements of polycrystalline samples were fulfilled by Faraday's method at room temperature and on a SQUID (Quantum Design) magnetometer at a temperature of 5 K in an external magnetic field of up to 40 kOe. To eliminate the effects of particle motion, the powder sample (~1 mg) was immobilized by ~10 mg of epoxy glue. At this weight ratio, during the measurements of the magnetization susceptibility, the diamagnetic contribution from the glue and the sample holder was about 0.01–0.001 of the contribution from the sample.

3. Results and discussion

3.1. Crystal structure

[**Pt–Co**] crystallizes in an orthorhombic cell (Table 1). Despite the structure of [**Pd–Co**] being very close to the platinum analog, it has a lower symmetry (monoclinic). The monoclinic angle is 134.11(1)°, approaching 135° which corresponds to the orthorhombic cell. In the orthorhombic setting, the parameter *a* of the unit cell is 7.095 Å, differing from the parameter *b* by only ±0.005 Å. Such a small difference can cause incorrect indexing of powder X-ray diffraction data, yielding a tetragonal unit cell. As this is the only considerable difference between the structures, which are generally very similar, we have discussed them together.

A general view of the unit cells is schematically presented in Fig. 2. The crystals of the DCS are built from isolated complex ions, shown in detail in Fig. 3. Mutual arrangement of the complex anions indicates that each complex ion is surrounded by six complex counter-ions. Therefore, the DCS crystallize in the distorted structural type of NaCl.

The cobalt atoms have an octahedral environment comprising of four oxygen atoms of the oxalate ligands (O_{ox}) and two oxygen atoms of coordinated water molecules (O_w). The Co–O_{ox} and Co–O_w distances (Table 2) differ by ±0.05 Å ([**Pt–Co**]) and 0.03 Å ([**Pd–Co**]), suggesting considerable non-equivalence in the strength of bonds made by the central atom to the monodentate and chelate ligands. Due to the rigidity of the chelate ions, the [CoO_6] octahedra are not regular – in the equatorial plane the adjacent angles deviate from 90°, being ~100° and 80°. The platinum/palladium atoms are square-coordinated with four nitrogen atoms. The adjacent angles between the M–N bonds are different from 90°, resulting in a slight distortion of the square planar cations.

As is evident from Fig. 2, there are two types of water molecules in the structure. Each cobalt atom coordinates to two water molecules in *trans* positions. Additionally, a pair of crystallization water molecules is present at each of the *ac* and *bc* faces of the unit cell. The molecules of the water of crystallization lie in the plane of the

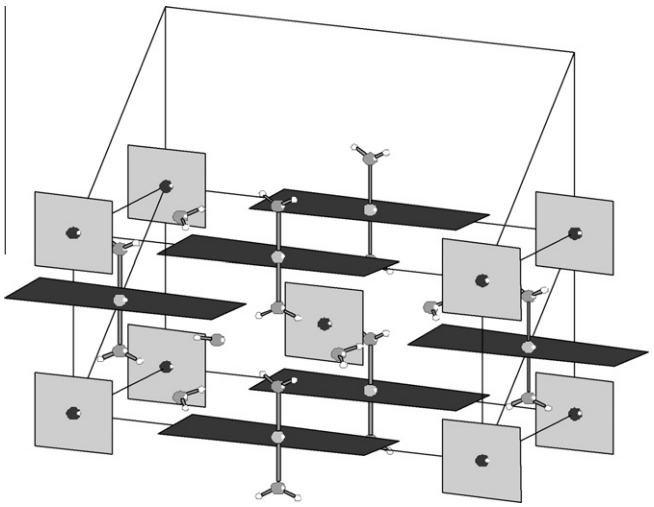

Fig. 2. General view of the unit cell of [**Pt–Co**]. The dashed lines designate the monoclinic setting of the [**Pd–Co**] unit cell.

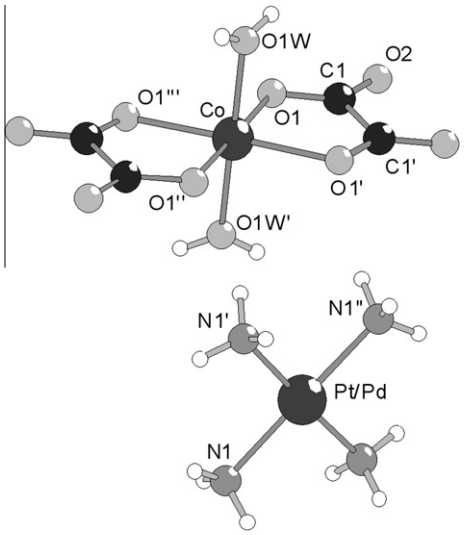

Fig. 3. Structure of the complex ions.

chelating ligands of the complex anions and form hydrogen bonds to the terminal oxygen atoms (O2). In turn, the coordinated water molecules are joined by hydrogen bonds with the crystallization water molecules. Thus, the crystallization water molecules and the complex cations are connected to the complex anions by a system of hydrogen bonds. The average O···O and O···N distances are 2.7 and 3.1 Å, which is characteristic of strong bonding in such systems. The list of the distances between the atoms A and D in the D–H···A system (Fig. 4 and Table 3) illustrates the situation.

As found with the powder X-ray diffraction, all precipitates of the compounds obtained are single-phase. Experimental diffraction patterns of the powder samples coincide with those calculated from the structural parameters, and do not have additional reflections.

3.2. Thermal properties in an inert atmosphere

In an inert atmosphere (helium), both DCS entirely decompose to form bimetallic phases. TG–DSC patterns and evolved gas curves, illustrating the release of the major gaseous products, are presented in Fig. 5. Both compounds decompose in two major steps, comprising, in turn, of several poorly separated stages. The first step corresponds to complete water loss. It is confirmed by the results of mass spectrometry. We suppose that the process of dehydration only weakly depends on the nature of the complex cation central atom, because the Pt/Pd atoms do not interact directly with water molecules, and the complex cations $[M(NH_3)_4]^{2+}$ have the same charge, shape and size. It is noteworthy that the TG curve of [**Pd–Co**] gives evidence that water removal occurs in two stages. In the first stage (temperature interval 80–120 °C) two hydration water molecules escape yielding the anhydrous salt $[Pd(NH_3)_4][Co(C_2O_4)_2(H_2O)_2]$. In the second stage (temperature interval 120–145 °C) two water molecules within the coordination sphere of the anion are removed, corresponding to $[Pd(NH_3)_4][Co(C_2O_4)_2]$ formation. The DSC curve exhibits two resolved endo effects. For [**Pt–Co**], the stages of removal of the hydration and coordinated water (85–150 °C) are not distinguished, and the DSC curve has one asymmetric endo effect. The measured average heats of dehydration are 202(±10%) kJ/mol ([**Pt–Co**]) and 192(±10%) kJ/mol ([**Pd–Co**]).

The second step corresponds to the complete decomposition of the complexes to bimetallic products. The starting temperatures for these processes are different: 190 °C ([**Pd–Co**]) and 240 °C ([**Pt–Co**]). As is known, palladium complex compounds are thermally less stable than the analogous complexes with platinum. For this reason, we believe that the difference in the thermal stability of the anhydrous products is primarily determined by the thermal stability of the complex cations $[M(NH_3)_4]^{2+}$. As one can see, the complete decomposition is followed by two endothermic effects for [**Pd–Co**] and by three for [**Pt–Co**]. In order to elucidate the mechanistic details of the thermal decomposition of [**Pt–Co**], it was heated in helium to preset temperatures, then the system was rapidly cooled (quenched), and the intermediate products were examined.

Heating to 260 °C (the maximum of the endo effect 2) yields the anhydrous DCS $[Pt(NH_3)_4][Co(C_2O_4)_2]$ (Fig. 6). Holding a sample at this temperature for 30 min is accompanied by continuous weight loss, indicating the thermal instability of the intermediate products. After heating to 300 °C (endo effect 3) only $[Pt(NH_3)_4][Co(C_2O_4)_2]$ and $[Pt(NH_3)_2C_2O_4]$ phases are observed in the thermolysis products. Apparently cobalt stands in the amorphous phase of CoC_2O_4. Heating to 330 °C (endo effect 4) affords a disordered solid solution of $Co_{0.3}Pt_{0.7}$ (a = 3.860(4) Å, V/Z = 14.38 Å^3, space group $Fm\bar{3}m$), with the pattern lacking reflections from other phases (Fig. 6). Most likely, some part of the non-reduced cobalt is amorphous, because further heating to 400 °C results in the formation of the single-phase disordered solid solution $Co_{0.5}Pt_{0.5}$ (a = 3.749(4) Å, V/Z = 13.17 Å^3, space group $Fm\bar{3}m$, Table 4).

A powder X-ray diffraction study of the thermolysis products obtained at different temperatures supports the hypothesis [29] that the decomposition of $[M(NH_3)_4][Co(C_2O_4)_2]$ proceeds by the following pathway:

(1) $[M(NH_3)_4][Co(C_2O_4)_2] \rightarrow [M(NH_3)_2C_2O_4] + CoC_2O_4 + 2NH_3$,
(2) $[M(NH_3)_2C_2O_4] \rightarrow M + 2NH_3 + 2CO_2$,
(3) $CoC_2O_4 \rightarrow Co + 2CO_2$.

As a result the process involving oxalate-ion oxidation occurs:

$$[M(NH_3)_4][Co(C_2O_4)_2] \rightarrow (Co + M) + 4CO_2 + 4NH_3 \quad (1)$$

However, the fact that the anhydrous DCS is present in the products of the thermal decomposition, until temperatures near total decay, as well as the presence of nitrogen and water in the evolving gases, a second parallel process involving ammonia oxidation is evident:

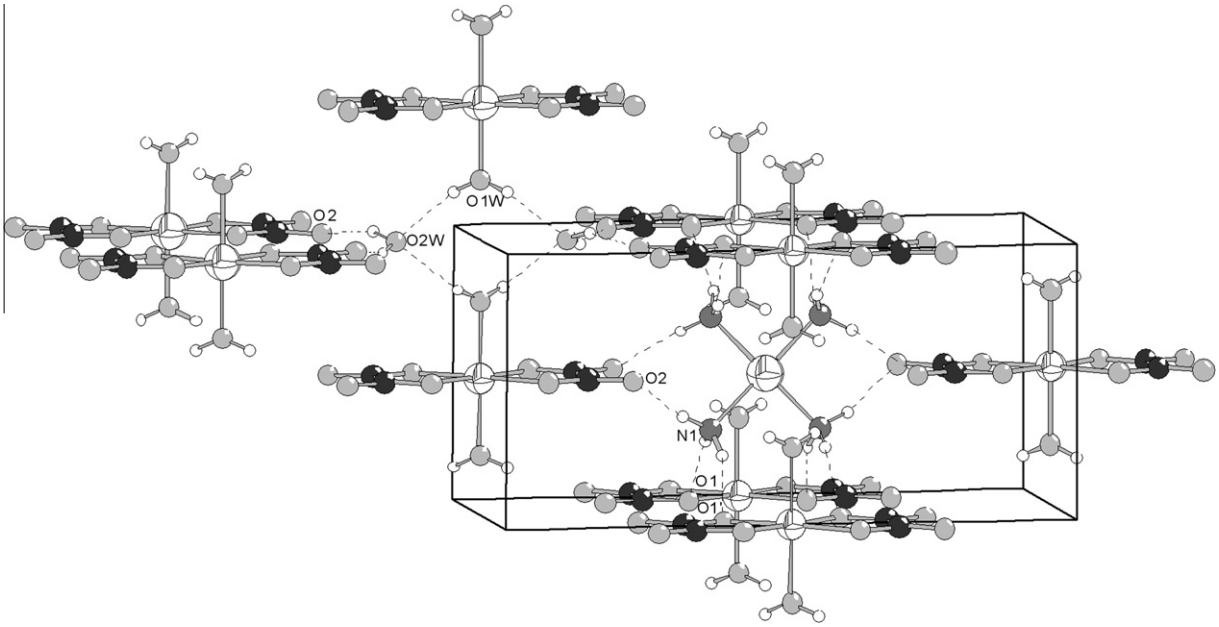

Fig. 4. Hydrogen bonding between structural units in the DCS.

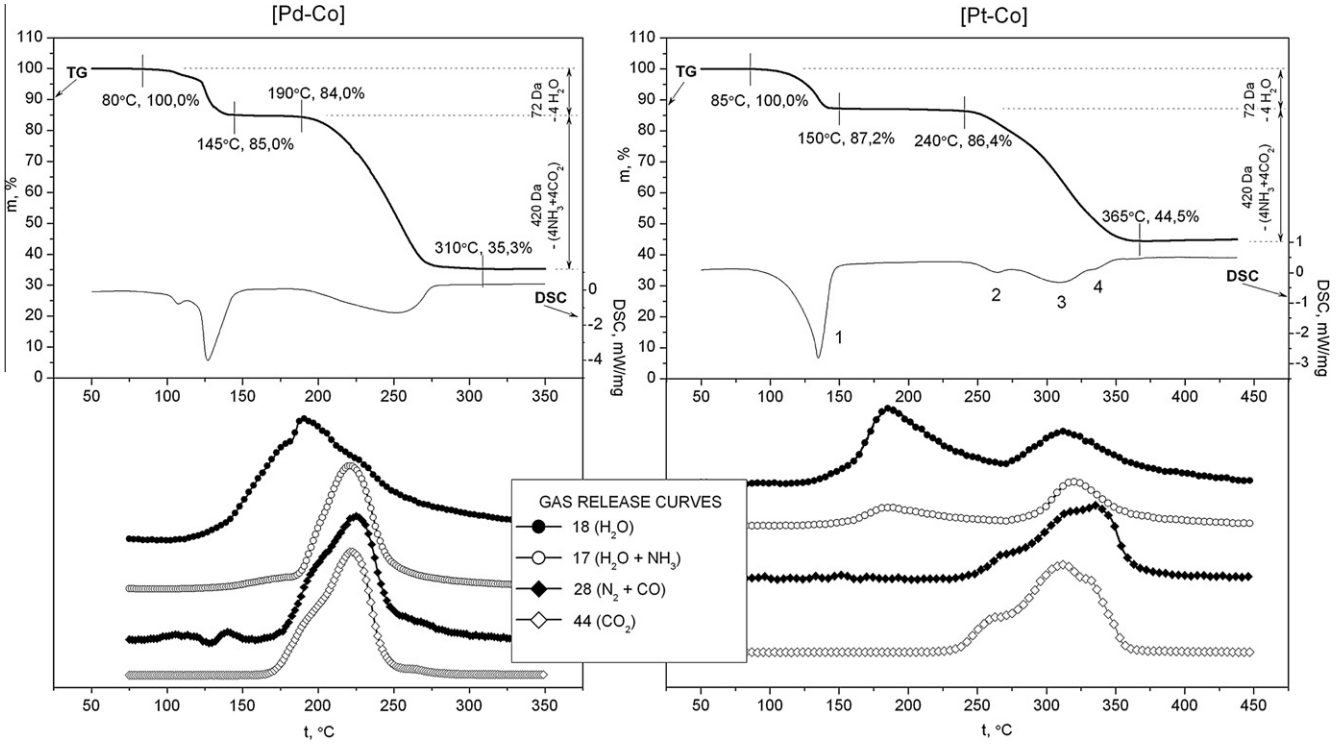

Fig. 5. Top – TG–DSC curves of DCS; bottom – profiles of gas release curves.

$$[M(NH_3)_4][Co(C_2O_4)_2] \rightarrow (Co + M) + 2CO_2 + 8/3NH_3 + 2/3N_2 + 2CO + 2H_2O \quad (2)$$

3.3. The products of DSC thermolysis in hydrogen

When heated in hydrogen at 200 °C, [**Pd–Co**] partially decomposes affording metallic palladium. Heating at 400 °C results in the formation of the solid solution $Pd_{0.5}Co_{0.5}$. A further increase in the annealing temperature up to 600 °C results only in crystallite growth. This result is in good agreement with the phase diagram Co–Pd. According to the phase diagram, palladium and cobalt form a continuous series of solid solutions [30,31].

Decomposition of [**Pt–Co**] under a hydrogen atmosphere (Fig. 7) proceeds in three steps. The first step (100–150 °C) corresponds to the removal of all four water molecules (72 Da) and affords anhydrous $[Pt(NH_3)_4][Co(C_2O_4)_2]$. In the second step (185–225 °C), the weight loss matches the escape of two ammonia molecules (34 Da), which may be indicative of the formation of two phases: $[Pt(NH_3)_2C_2O_4]$ and CoC_2O_4, as was observed in a helium atmo-

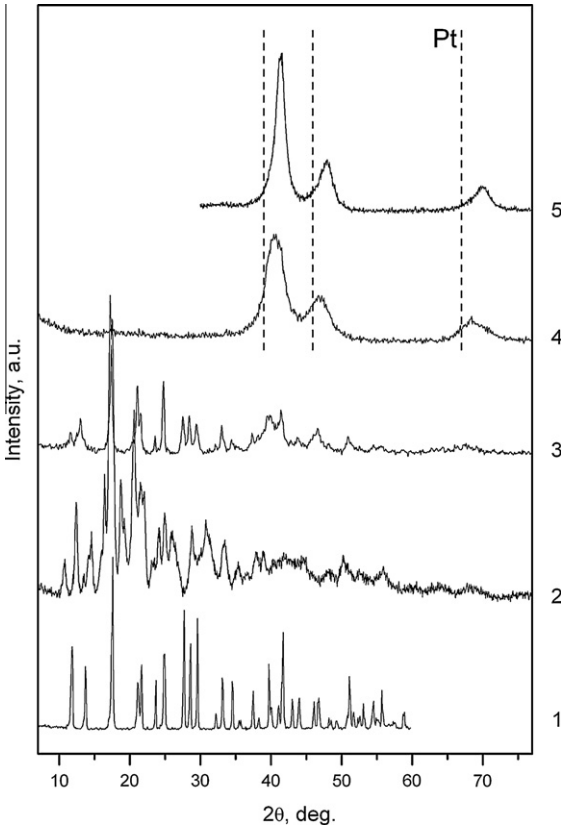

Fig. 6. XRD powder patterns of [**Pt–Co**] thermolysis products in a He atmosphere: 1 – the initial [**Pt–Co**]; 2 – the anhydrous $[Pt(NH_3)_4][Co(C_2O_4)_2]$ (260 °C); 3 –mixture of $[Pt(NH_3)_4][Co(C_2O_4)_2]$ and $[Pt(NH_3)_2C_2O_4]$ (300 °C); 4 – $Co_{0.3}Pt_{0.7}$ random solid solution (330 °C); 5 – $Co_{0.5}Pt_{0.5}$ random solid solution (400 °C). Dashed lines denote maxima of pure platinum diffraction peaks.

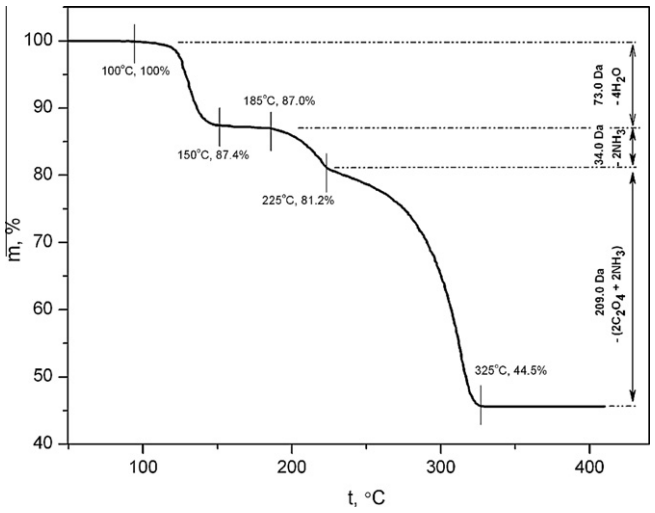

Fig. 7. TG curve of [**Pt–Co**] in a hydrogen atmosphere.

sphere. But, according to XRD data, heating of [**Pt–Co**] at 200 °C leads to incomplete reduction and yields platinum (Fig. 8). The diffraction pattern exhibits reflections of pure platinum and anhydrous DCS. Full reduction occurs at 325 °C, yielding a disordered solid solution $Co_{0.5}Pt_{0.5}$ (Table 4), while the phase diagram of the system predicts that below 820 °C, the equilibrium phase is the ordered CoPt intermetallic, which has a tetragonal lattice (CuAu type, space group *P*4/*mmm*).

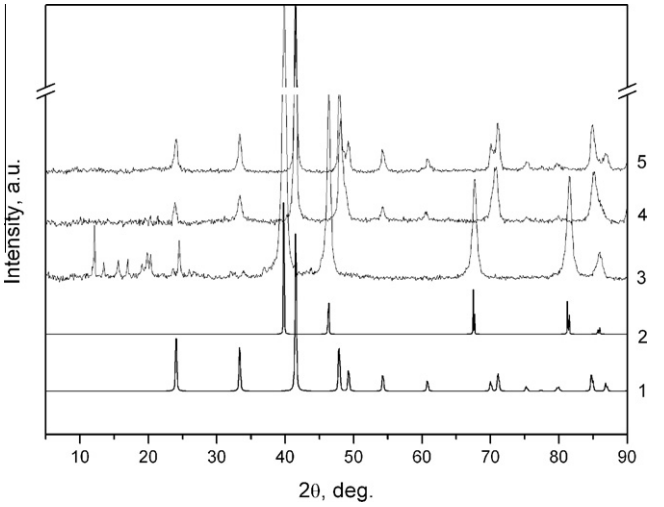

Fig. 8. XRD powder patterns of [**Pt–Co**] thermolysis products in a H_2 atmosphere: 1 – the reference samples of CoPt intermetallic (JCPDF 65-8969); 2 – the reference sample of pure platinum (JCPDF 4-802); 3 – sample of DCS heated up to 200 °C. There are the initial DCS and platinum peaks; 4 – partly ordered $Co_{0.5}Pt_{0.5}$ solid solution, the order parameter α is 45% (400 °C); 5 – highly ordered CoPt intermetallic (600 °C).

According to the SEM and HRTEM microphotographs, the morphology of the conglomerates of metallic particles for this specimen inherits the habitus of the crystals of the initial DCS. However, scans with increasing resolution reveal that the conglomerates are built from smaller particles with sizes of about 10 nm (Fig. 9).

In order to examine the chemical ordering dynamics in $Co_{0.5}Pt_{0.5}$ solid solutions, a series of annealing experiments was carried out at varying temperatures. In each of the experiments, a fresh sample of the starting [**Pt–Co**] was heated in a reactor to the preset temperature at the rate of 10 K/min in hydrogen, and then exposed to this temperature for 1 h. The sample was then cooled in helium and the powder diffraction pattern was recorded at room temperature.

To calculate the order parameter α of the solid solution, the following technique was used. For each of the experimental patterns, the corresponding theoretical pattern of the $Co_{0.5}Pt_{0.5}$ sample was calculated with different site occupation factors p for the cobalt and platinum atoms (Fig. 10). Occupation factors of the structural positions with the two atoms in the CoPt intermetallic (for 1a structural positions: Co $p = x$, Pt $p = 1 - x$ and for 1d – Pt $p = x$, Co $p = 1 - x$, where p may change from 0.5 for a random solid solution to 1 for an intermetallic) were refined by the full-profile method. When the patterns matched, the obtained value of p was put in the formula $\alpha = 2(p - 0.5) \times 100\%$.

The sample obtained at 400 °C is the solid solution $Co_{0.5}Pt_{0.5}$ with an order parameter of 15% (Table 4). An increase in temperature up to 600 °C improves the order parameter to 70%. The XRD pattern of the sample annealed at 800 °C shows superstructure reflections with intensities corresponding to complete ordering ($\alpha = 100\%$) in the CoPt intermetallic. A further increase of the annealing temperature to 850 °C (the temperature of the order–disorder phase transition is 825 °C) affords the disordered solid solution $Co_{0.5}Pt_{0.5}$ ($a = 3.749(1)$ Å, $V/Z = 13.17$ Å^3, space group $Fm\bar{3}m$, Table 4), with particle sizes of about 16–21 nm.

3.4. Magnetic measurements

The measurements of magnetization versus external field afforded dependencies characteristic of soft ferromagnets (Fig. 11). The main parameters, determined at 5 K and at room temperature, are

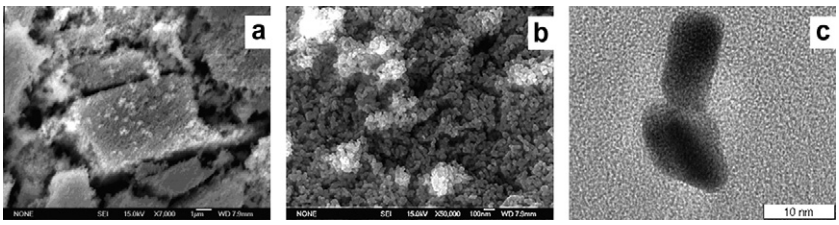

Fig. 9. SEM (a, b) and HRTEM (c) microphotographs of CoPt particles obtained at 400 °C. (a) The shape of metal particles conglomerates inherits a habitus of crystals of the initial [**Pt**–**Co**]. Increasing the resolution reveals the conglomerates consist of smaller particles which are about 10 nm in size (b, c).

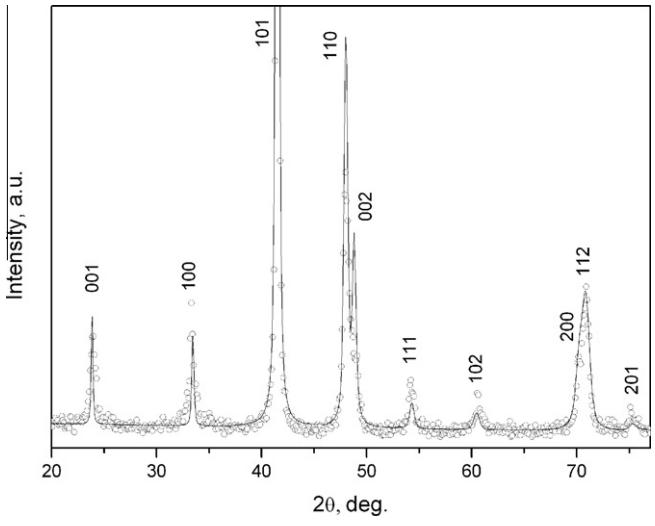

Fig. 10. Comparison of the experimental XRD powder pattern of partly ordered $Co_{0.5}Pt_{0.5}$ solid solution obtained by reduction of [**Pt**–**Co**] in a H_2 atmosphere and annealing at 400 °C for 1 h, and the theoretical diffraction pattern calculated for the order parameter (α) 15%.

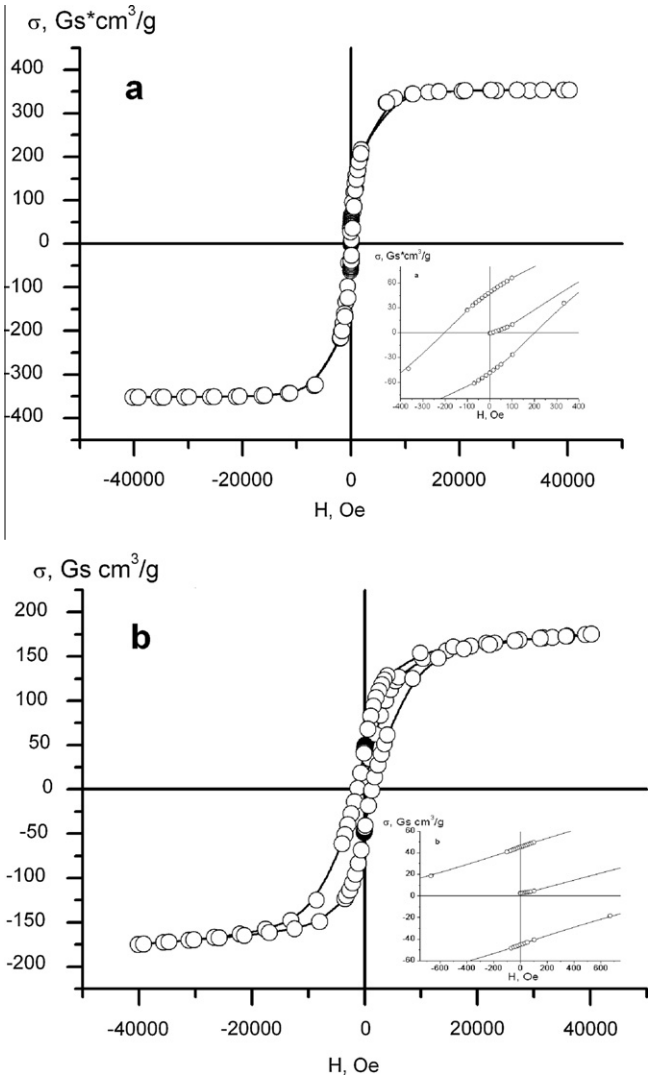

Fig. 11. Hysteresis loops of $Co_{0.5}Pd_{0.5}$ (a) and $Co_{0.5}Pt_{0.5}$ (b) nanoparticles measured at 5 K.

listed in Table 5. The values given in the table are scaled to the weight content of cobalt in the sample of the solid solution. Saturation magnetization of all samples is less than that of hexagonal close-packed bulk cobalt ($\sigma_s \approx 162$ Gs cm^3/g) [32]. This fact, apparently, is related to the presence of a thin layer of antiferromagnetic cobalt oxide on the surface of the nanoparticles.

The measurements of the magnetic moment (σ) at 5 K make it possible to extrapolate the values to σ_∞, corresponding to zero temperature and infinite magnetic field. Thus, magnetic moment per cobalt atom can be estimated: $Co_{0.5}Pd_{0.5}$ – 2.5 BM, $Co_{0.5}Pt_{0.5}$ – 2.0 BM.

The ratio σ_r/σ_s for both samples (0.15 for $Co_{0.5}Pd_{0.5}$ and 0.25 for $Co_{0.5}Pt_{0.5}$) indicate the quasi single-domain state of the particles [33], being in good accordance with their characteristic size. The low coercive force H_c of the $Co_{0.5}Pd_{0.5}$ sample suggests larger particle sizes. Such particles are magnetized through the movement of domain walls. On the contrary, in the $Co_{0.5}Pt_{0.5}$ sample, the size of the particles is closer to the upper boundary of the single-domain region. Therefore, the main process is the rotation of the magnetic moments of the particles around the easy axis, which requires a relatively larger energy. As a result, H_c amounts to approximately 1 kOe.

Table 5
Main parameters of the magnetization curve.

Sample	T (K)	Saturation magnetization, σ_s (Gs cm^3/g)	Remanence, σ_r (Gs cm^3/g)	Coercitivity, H_c (Oe)
$Co_{0.5}Pd_{0.5}$	5	350	50	200
$Co_{0.5}Pt_{0.5}$	5	170	45	1270
$Co_{0.5}Pd_{0.5}$	298	160	110	60
$Co_{0.5}Pt_{0.5}$	298	90	60	400

4. Conclusion

Crystal structures of DCS $[M(NH_3)_4][Co(C_2O_4)_2(H_2O)_2]\cdot 2H_2O$ (M = Pd, Pt) were determined for the first time by single crystal X-ray diffraction. Mechanistic details of decomposition of the studied [**Pd**–**Co**] and [**Pt**–**Co**] in helium have been revealed. It has been

found that the process is rather complicated and is governed by two parallel processes. It is been demonstrated that the DCS in question are promising precursors of $Co_{0.5}Pd_{0.5}$ and $Co_{0.5}Pt_{0.5}$ nanoalloys. Thermal decomposition of the prepared DCS in helium affords face-centered cubic random solid solutions of $Co_{0.5}Pd_{0.5}$ and $Co_{0.5}Pt_{0.5}$ with crystallite sizes of 5–8 nm as the final products.

As evidenced by X-ray diffraction data, on reduction of the starting DCS in hydrogen, metal atoms of the anionic and cationic spheres have escape separately in time. First, the platinum metal is reduced (to Pd or Pt), then the Co atoms emerge, which penetrate into the structure of the nuclei formed and afford the solid solution of $Co_{0.5}M_{0.5}$, with crystallite sizes 7–21 nm.

Variation of the thermal treatment of the thermolysis products of [**Pt**–**Co**] allows the preparation of $Co_{0.5}Pt_{0.5}$ solid solutions having different order parameters, while the crystallite size shows a slight alteration. Thus, a random solid solution $Co_{0.5}Pt_{0.5}$ ($a = 3.749(4)$ Å, $V/Z = 13.17$ Å^3, crystallite size 7–9 nm) was obtained at 325 °C, while at 800 °C – CoPt intermetallic was obtained ($a = 2.682(2)$ Å, $c = 3.675(3)$ Å, $V/Z = 13.25$ Å^3, crystallite size 16–21 nm).

Acknowledgements

This work has been partially supported by RFBR Grant 11-03-00668-a, Presidium SB RAS interdisciplinary project No. 112, State contracts No. P960 of Federal target program "Scientific, Research And Teaching Specialists In Russia" 2009–2013 and GC No. 02.740.11.0628 of FFP "SSESIR 2009–2013".

Appendix A. Supplementary data

CCDC 420432 and 420437 contains the supplementary crystallographic data for [**Pd**–**Co**] and [**Pt**–**Co**]. These data can be obtained free of charge via http://www.ccdc.cam.ac.uk/conts/retrieving.html, or from the Cambridge Crystallographic Data Centre, 12 Union Road, Cambridge CB2 1EZ, UK; fax: (+44) 1223-336-033; or e-mail: deposit@ccdc.cam.ac.uk.

References

[1] N. Toshima, T. Yonezawa, New J. Chem. (1998) 1179.
[2] F. Tournus, A. Tamion, N. Blanc, A. Hannour, L. Bardotti, B. Prével, P. Ohresser, E. Bonet, T. Epicier, V. Dupuis, Phys. Rev. B77 (2008) 144411.
[3] L. Gutierrez, A. Boix, E.A. Lombardo, J. Fierro, J. Catal. 199 (2001) 60.
[4] Q.-S. Chen, S.-G. Sun, Z.-Y. Zhou, Y.-X. Chen, S.-B. Deng, Phys. Chem. Chem. Phys. 10 (2008) 3645.
[5] W. Mustain, K. Kepler, J. Prakash, Electrochem. Commun. 8 (2006) 406.
[6] M. Tarasevich, A. Chalykh, V. Bogdanovskaya, L. Kuznetsova, N. Kapustina, B. Efremov, M. Ehrenburg, L. Reznikova, Electrochim. Acta 51 (21) (2006) 4455.
[7] M. Tarasevich, V. Bogdanovskaya, L. Kuznetsova, A. Modestov, B. Efremov, A. Chalykh, Yu. Chirkov, N. Kapustina, M. Ehrenburg, J. Appl. Electrochem. 37 (2007) 1503.
[8] V. Tzitzios, D. Niarchos, G. Margariti, J. Fidler, D. Petridis, Nanotechnology 16 (2005) 287.
[9] S. Jeong, Y.-N. Hsu, D. Laughlin, M. McHenry, IEEE Trans. Magn. 36 (2000) 2336.
[10] D. Crew, L. Lewis, J. Kim, K. Barmak, J. Appl. Phys. 89 (2001) 7528.
[11] J.-B. Ding, D.-H. Qin, Y. Huang, L. Cao, H.-L. Li, J. Mater. Eng. Perform. 12 (2003) 584.
[12] T. Ould Ely, C. Pan, C. Amiens, B. Chaudret, F. Dassenoy, P. Lecante, M.-J. Casanove, A. Mosset, M. Respaud, J.-M. Broto, J. Phys. Chem. B 104 (2000) 695.
[13] J.-I. Park, M. Kim, Y.-W. Jun, J. Lee, W.-R. Lee, J. Cheon, J. Am. Chem. Soc. 126 (2004) 9072.
[14] Manju Lata Rao, S. Sundar Manoharan, D. Elefant, C. Schneider, J. Nanosci. Nanotechnol. 4 (2004) 722.
[15] J.-I. Park, J. Cheon, J. Am. Chem. Soc. 123 (24) (2001) 5743.
[16] W. Yong, Y. Hong, J. Am. Chem. Soc. 127 (2005) 5316.
[17] M.A. Willard, L.K. Kurihara, E.E. Carpenter, S. Calvin, V.G. Harris, Int. Mater. Rev. 49 (3–4) (2004) 125.
[18] V. Tzitzios, D. Niarchos, G. Margariti, J. Fidler, D. Petridis, Nanotechnology 16 (2005) 287.
[19] K. Yusenko, E. Filatov, D. Vasilchenko, I. Baidina, A. Zadesenez, Yu. Shubin, Z. Kristallogr. Suppl. 26 (2007) 289.
[20] A. Zadesenets, E. Filatov, K. Yusenko, Yu. Shubin, S. Korenev, I. Baidina, Inorg. Chim. Acta 361 (2008) 199.
[21] I. Chernyaev, Synthesis of Complex Compounds of Platinum Group Metals, Nauka, Moscow, 1964.
[22] G.M. Sheldrick, Acta Crystallogr. A64 (2008) 112.
[23] PCPDFWin, V. 1.30, JCPDS ICDD, Swarthmore, PA, USA, 1997.
[24] W. Kraus, G. Nolze, POWDERCELL 2.4, Program for the Representation and Manipulation of Crystal Structures and Calculation of the Resulting X-ray Powder Patterns, Federal Institute for Materials Research and Testing, Berlin, Germany, 2000.
[25] S. Krumm, Mater. Sci. Forum 183 (1996) 228.
[26] E. Gebhardt, W. Koster, Z. Metallkd. 32 (1940) 253.
[27] M. Heibel, G. Kumar, C. Wyse, P. Bukovec, A. Bocarsly, Chem. Mater. 8 (1996) 1504.
[28] Netzsch Proteus Thermal Analysis v.4.8.1., Netzsch-Gerätebau, Bayern, Germany, 2005.
[29] M.L. Blokhina, A.I. Blokhin, M.Ya. Nikulin, M.G. Derikova, Powder Metall. Met. Ceram. 35 (1996) 118.
[30] T.B. Massalski (Ed.), Binary Alloy Phase Diagrams, vol. 1225, ASM International, Materials Park, Ohio, 1990.
[31] T.B. Massalski (Ed.), Binary Alloy Phase Diagrams, second ed., vol. 1220, ASM International, Materials Park, Ohio, 1990.
[32] J.R. Childress, C.L. Chien, Phys. Rev. B 43 (1991) 8089.
[33] D. Srikala, V.N. Singh, A. Banerjee, et al., J. Nanosci. Nanotechnol. 9 (9) (2009) 5627.